

# The Distribution of H<sub>2</sub>O Maser Emission in the Nucleus of NGC 4945

L. J. Greenhill, J. M. Moran, & J. R. Herrnstein<sup>1</sup>

Harvard-Smithsonian Center for Astrophysics, 60 Garden St, Cambridge, MA 02138

Received \_\_\_\_\_; accepted \_\_\_\_\_

*To appear in Ap.J. (Letters)*

arXiv:astro-ph/9702220v1 25 Feb 1997

---

<sup>1</sup>Currently at the National Radio Astronomy Observatory, Socorro, NM 87801

## ABSTRACT

We present the first interferometer map of the H<sub>2</sub>O maser emission in the active nucleus of NGC 4945, which exhibits both starburst and Seyfert qualities. Although the declination of the galaxy is  $-49^\circ$ , we were able to make the observations with the southernmost antennas of the Very Long Baseline Array. Strong maser emission is present in three velocity ranges, one near the systemic velocity and two shifted roughly symmetrically by  $\pm(100 - 150) \text{ km s}^{-1}$ . This is the first detection of highly blue-shifted water emission in NGC 4945. We also report a marginal detection of previously unreported red-shifted emission at a velocity of  $\sim +200 \text{ km s}^{-1}$  with respect to systemic. From fringe rate analysis we determined the position of the maser to be  $\alpha_{1950} = 13^h 02^m 32^s 28 \pm 0^s 02$ ;  $\delta_{1950} = -49^\circ 12' 01'' 9 \pm 0'' 1$ . The uncertainties in earlier estimates are at least several arcseconds. The maser lies within  $2''$  (36 pc at a distance of 3.7 Mpc) of the peaks in 1.4 GHz continuum and 1.6  $\mu\text{m}$  emission from the nucleus. The mappable maser emission is distributed roughly linearly over  $\approx 40$  milliarcseconds (0.7 pc) at a position angle of  $\approx 45^\circ$ , which is close to the  $43 \pm 2^\circ$  position angle of the galactic disk. The red and blue-shifted emission symmetrically straddle the systemic emission on the sky, which suggests material in edge-on circular motion around a central object. The position-velocity structure indicates a binding mass of  $\sim 1 \times 10^6 M_\odot$ , within a volume of radius  $\approx 0.3$  pc, which in combination with estimates of the AGN luminosity, implies that the central engine radiates on the order of 10% of its Eddington luminosity.

*Subject headings:* galaxies: individual, NGC 4945 — galaxies: kinematics and dynamics — galaxies: nuclei — masers

## 1. Introduction

The edge-on spiral galaxy NGC 4945 contains the first H<sub>2</sub>O maser discovered in a galactic nucleus (dos Santos & Lépine 1979; Batchelor, Jauncey, & Whiteoak 1982). Within the nucleus there is a heavily absorbed hard X-ray component ( $> 10$  keV), with a measured column density of  $n_H = 5 \times 10^{24} \text{ cm}^{-2}$  (Iwasawa et al., 1993), and true X-ray luminosity (2–20 keV) of  $9 \times 10^{41} \text{ erg s}^{-1}$ . The hard component varies on timescales of hours, implying a source size of  $\sim 10^{15} \text{ cm}$ . The nucleus is very prominent at infrared wavelengths, with a far infrared luminosity  $L_{\text{FIR}} = 2 \times 10^{43} \text{ erg s}^{-1}$  from the inner 200 pc (Brock et al., 1988), at an assumed distance of 3.7 Mpc (Whiteoak & Wilson 1990). The nucleus also shows a  $\sim 1 \times 6$  kpc ionization cone along the galactic minor axis (Nakai 1989) and emission knots with LINER-like spectra (Moorwood et al., 1995). Optical line splittings of up to  $600 \text{ km s}^{-1}$  (Heckman, Armus, & Miley 1990, Moorwood et al., 1995) indicate that the cone is evacuated by a nuclear wind. While X-ray characteristics suggest that the active galactic nucleus (AGN) is driven by an obscured Seyfert nucleus, the high IR luminosity and wind indicate the presence of a nuclear starburst.

Spectra of the maser consistently show emission ( $\sim 1 \text{ Jy}$ ) within about  $\pm 20 \text{ km s}^{-1}$  of the systemic velocity and stronger emission ( $\sim 5 - 10 \text{ Jy}$ ) red-shifted by  $\sim 100 - 150 \text{ km s}^{-1}$  (e.g., Whiteoak & Gardner 1986, Figure 1). Previously, no corresponding emission on the blue side of the systemic velocity has been detected (e.g., Nakai et al., 1995). We adopt a heliocentric systemic velocity of  $561 \pm 4 \text{ km s}^{-1}$ , based on CO observations (Dahlem et al., 1993). (Velocities are defined with respect to the standard radio astronomical definition of Doppler shift throughout.) The importance of nuclear H<sub>2</sub>O masers to the study of AGN has been widely appreciated after recent observations of the maser in the nucleus of NGC 4258 (Miyoshi et al., 1995), where the masers were found to trace a thin molecular Keplerian disk of 0.13 pc inner radius around a central mass of  $3.6 \times 10^7 M_\odot$ . In this Letter,

we report the first sub-arcsecond estimate of the maser position in NGC 4945, the detection of blue-shifted maser features, and the first interferometric map of the distribution of maser emission.

## 2. Observations & Results

We observed the maser with the Very Long Baseline Array of the NRAO<sup>1</sup> for 4 hours

---

<sup>1</sup> The National Radio Astronomy Observatory is operated by Associated Universities, Inc, under cooperative agreement with the National Science Foundation.

---

on 1995 January 22. We used the southernmost stations, at Mauna Kea, HI (MK), Saint Croix, VI (SC), and Kitt Peak, AZ (KP). At KP the source reached a maximum elevation of  $8.6^\circ$ , while it was  $11^\circ$  and rising at MK. We obtained useful data for only 2.5 hours on the MK–KP baseline. Observing conditions at Saint Croix were relatively poor and no useful data were obtained from it. Tipping scans showed that the opacity at KP, MK, and SC were 0.07, 0.05, and 0.3 at zenith, respectively. The baseline length was 4470 km and the angular resolutions were  $\sim 0.6$  and  $\sim 1.8$  milliarcseconds (mas) in right ascension and declination, respectively. The system temperatures for  $8^\circ$  elevation at KP and MK were 170 and 130 K, respectively. We recorded four contiguous bandpasses covering the range  $405 \text{ km s}^{-1}$  to  $821 \text{ km s}^{-1}$ , so as to include the systemic emission, the red-shifted emission, and the likely velocity range of counterpart blue-shifted emission. The spectrum is shown in Figure 1.

We calibrated the data with the NRAO AIPS package. The interferometer delays and

fringe rates were estimated from observations of the continuum sources 4C39.25, 3C273, and 1147 – 382. The latter source was observed at elevations  $< 20^\circ$  and was included so that we could estimate the magnitude of elevation dependent errors in the correlator model and post-correlation analysis. The delay calibration is accurate to about 3 ns overall, after implementing the U. S. Naval Observatory station positions and earth orientation parameters (Eubanks, private communication).

We analyzed the fringe rate of the maser emission as a function of time to estimate the position of the maser, taking into account the effect of the atmosphere. We fit a sinusoid to the measured fringe rates for emission between 664 and 719  $\text{km s}^{-1}$  (with uniform weighting) to obtain position offsets of  $+2.7''$  and  $+8.2''$  from the *a priori* position  $\alpha_{1950} = 13^h 02^m 32^s 000$ ,  $\delta_{1950} = -49^\circ 12' 10'' 05$ , with respect to a reference frame consisting of the sources 4C39.25, 1147 – 382, and 3C273B. We conservatively estimate the uncertainties in position based on the residual fringe rates of the maser and calibrator sources. The new maser position is

$$\alpha_{1950} = 13^h 02^m 32^s 28 \pm 0^s 02, \delta_{1950} = -49^\circ 12' 01'' 9 \pm 0'' 1;$$

$$\alpha_{2000} = 13^h 05^m 27^s 48 \pm 0^s 02, \delta_{2000} = -49^\circ 28' 05'' 4 \pm 0'' 1.$$

To map the brightness distribution of the maser, we phase referenced the data to the strong spectral feature at  $699 \pm 0.8 \text{ km s}^{-1}$ . The phases of this feature were subtracted from the phases of other spectral features, which corrected for the effects of the atmosphere and calibration uncertainties. We assumed a point source model and fit a sinusoid (of 24 hour period) to the difference phase, estimating relative feature positions and formal errors (e.g., Thompson, Moran, & Swenson 1986). Sample phase plots are shown in Figure 2. The data were averaged in frequency across the line profile for each feature and averaged in time for between 300 s and 640 s so that phase ambiguities could be resolved prior to fitting. For

a 1 Jy feature that is  $1 \text{ km s}^{-1}$  wide (half power width) the signal-to-noise ratio in 300 s is about 4.

The structure of the maser is remarkably linear, with emission distributed over  $\approx 40$  mas between  $414$  and  $719 \text{ km s}^{-1}$  (Figure 3). Deviations from linearity are antisymmetric with respect to the systemic emission, which gives the appearance of a shallow “S” on the sky. The centroids of the blue and red emission are separated by  $\approx 30$  mas or  $0.55 \text{ pc}$ , at a position angle of  $\approx 45^\circ$ , and roughly symmetrically bracket the systemic emission. The wide separations among the systemic, red, and blue emission correspond to many interferometer fringes and are well determined. Maser features that are detected only marginally (i.e., with a rms of residuals about the fitted model of  $> 1 \text{ rad}$ ) are not shown in the map, although they do not appreciably alter the source structure. These marginal features include one at  $\approx 779 \text{ km s}^{-1}$ , which is more red-shifted than any previously reported maser emission in NGC 4945. In Nonetheless, not all of the detected maser features could be mapped, particularly near the systemic and blue-shifted velocities, because a significant fraction are not well approximated by a point source model (i.e., the phases could not be fit by a diurnal sinusoid).

The interferometer calibration was sufficiently good that uncertainty in the astrometric position of the maser is the largest source of quantifiable systematic error in estimating maser feature positions. The error is  $\lesssim 90 \mu\text{as}$ , which is computed for an astrometric uncertainty of  $100 \text{ mas}$  and for a feature  $200 \text{ km s}^{-1}$  from the reference, and is proportional to both quantities. (Residual atmospheric delay contributes a moderate systematic error because of the low elevations at which we observed the maser; it is smaller than the error from the astrometry.) A second source of systematic error arises from the possibility that emission, for each feature, may not be well described by a point source, which is difficult to quantify. However, the data for each mapped maser feature is well fit by a point source

model over the limited range of hour angle available. The systematic error in position for each maser feature is less than the statistical error, which is dominated by the limited range of hour angle over which the phases were measured. This limitation leads to 1) a large correlation between right ascension and declination parameters and 2) an uncertainty as to in which lobe of the interferometer fringe pattern the maser lies. Uncertainties in the estimated positions take into account possible lobe ambiguities.

### 3. Discussion

The new astrometric position of the maser clearly shows that it is associated with the center of the galactic nucleus (Figure 5). The previous position of Batchelor et al., (1982), obtained with the Parkes antenna of the CSIRO, was substantially more uncertain because of the beamwidth of the antenna. The maser lies within  $1\sigma$  of the infrared peak at  $1.6 \mu\text{m}$  and overlaps the radio continuum source, which Whiteoak & Wilson (1990) estimate is  $6'' \times 2''$  in size at 6 GHz (see Figure 5).

We cautiously interpret the data for the maser in NGC 4945 in terms of the paradigm established for NGC 4258. The extensive data on NGC 4258, with its clear Keplerian signature, show that the masers define a nearly edge on thin annular disk. The data for NGC 4945 are more sketchy but they share the characteristic of systemic emission bracketted roughly symmetrically in velocity *and* position by high-velocity emission. Moreover, the angular distributions of blue-shifted emission is roughly linear and the velocities decline with angular distance from the systemic emission. However, the position errors are significant, the red-shifted emission does not appear to mirror this structure, the decline in velocity for the blue-shifted emission is faster than what is characteristic for a Keplerian rotation curve, and the non-point source emission that seems to exist at some systemic and blue-shifted velocities could not be mapped (Figure 4). Nonetheless, there is a suggestion that the

structures of NGC 4945 and NGC 4258 may be similar, and we proceed on that assumption.

In the context of an edge-on disk, the observations suggest a binding mass (for circular orbits) of  $M = 1.1V^2 D_{\text{Mpc}} b_{\text{mas}} \csc^2 i \csc^3 \theta$ , where  $M$  is the enclosed mass in units of  $M_{\odot}$ ,  $V$  is the orbital velocity in units of  $\text{km s}^{-1}$ ,  $D_{\text{Mpc}}$  is the distance in Mpc,  $b_{\text{mas}}$  is the radius in mas,  $i$  is inclination, and  $\theta$  is the azimuthal angle of the red-shifted masers in the disk plane ( $90^\circ$  is the plane of the sky). The binding mass is  $M \approx 1.4 \times 10^6 M_{\odot}$  for  $V = 150 \text{ km s}^{-1}$ ,  $b = 15 \text{ mas}$  or  $0.3 \text{ pc}$ , and  $i = \theta = 90^\circ$  (Figure 4). The implied mass density is  $\sim 1.6 \times 10^7 M_{\odot} \text{ pc}^{-3}$ . The position angle of the disk,  $\approx 45^\circ$ , is comparable to the position angle of the larger galactic disk,  $43 \pm 2^\circ$ , and the senses of rotation of the two disks are the same. If the observed  $9 \times 10^{41} \text{ erg s}^{-1}$  X-ray luminosity (Iwasawa et al., 1993) implies a bolometric luminosity on the order of  $10^{43} \text{ erg s}^{-1}$ , then the central engine radiates 10% of its Eddington luminosity. We note that the shallow “S” the mappable maser emission traces may be consistent with a warp in the disk, which could be caused by radiation-driven torques that result from oblique illumination by the central engine (Maloney, Begelman, & Pringle 1996), though this is not a definitive explanation.

The interpretation of the observed maser structure is not unique and radically different interpretations might be viable. The emission could arise from a complex of star forming regions superposed on or within the nucleus, or from jet-induced shocks in the AGN. The linear extent of the maser is comparable to galactic star formation complexes (e.g., W49N), although the velocity difference between the systemic and red-shifted features is large for adjacent star forming regions. Maser emission can arise in warm gas behind dissociative shocks (Elitzur, Hollenbach, & McKee 1989) and nondissociative shocks (Kaufman & Neufeld 1996), although the maser spectrum mandates a complex line-of-sight velocity structure for the shocks.

Interferometric synthesis observations will undoubtedly clarify the dynamical



characteristics of the maser region, providing a comprehensive map of the maser emission within  $200 \text{ km s}^{-1}$  of the systemic velocity. The dual nature of the nucleus, as both a starburst and a very heavily obscured Seyfert object, makes this water maser source particularly important since it may be used to probe the dynamics and structure of the nucleus on sub-parsec scales.

We thank P. Diamond for his assistance with aspects of the post-correlation processing, and S. Ellingsen for assistance in obtaining a spectrum of the maser at Parkes.

## REFERENCES

- Ables, J. G., et al., 1987, MNRAS, 226, 157
- Batchelor, R. A., Jauncey, D. A., & Whiteoak, J. B. 1982, MNRAS, 200, 19P
- Brock, D., Joy, M., Lester, D. F., Harvey, P. M., & Ellis, H. B. 1988, ApJ329, 208
- Dahlem, M., Golla, G., Whiteoak, J. B., Wielebinski, R., Hüttemeister, S., & Henkel, C.  
1993, A&A, 270, 29
- dos Santos, P. M., & Lépine, J. R. D. 1979, Nature, 278, 34
- Elitzur, M., Hollenbach, D. J., & McKee, C. F., 1989, ApJ, 346, 983
- Heckman, T. M., Armus, L., & Miley, G. K. 1990, ApJS, 74, 833
- Iwasawa, K., et al., 1993, ApJ, 409, 155
- Kaufman, M. J., & Neufeld, D. A. 1996, ApJ, 456, 250
- Large, M. I., Mills, B. Y., Little, A. G., Crawford, D. F., & Sutton, J. M. 1981, MNRAS,  
194, 693
- Maloney, P. R., Begelman, M. C., & Pringle, J. E. 1996, ApJ, 472, 582
- Miyoshi, M., Moran, J. M., Herrnstein, J. R., Greenhill, L. J., Nakai, N., Diamond, P. J., &  
Inoue, M. 1995, Nature 373, 127
- Moorwood, A. F. M. van der Werf, P. P., Kotilainen, J. K., Marconi, A., & Oliva, E. 1995,  
A&A, 308, L1
- Nakai, N. 1989, PASJ, 41, 1107
- Nakai, N., Inoue, M., Miyazawa, K., Miyoshi, M., & Hall, P. 1995, PASJ, 47, 771

Thompson, A. R., Moran, J. M., & Swenson, G. W. 1986, *Interferometry and Synthesis in Radio Astronomy*, (New York: Wiley)

Whiteoak, J. B., & Gardner, F. F. 1986, *MNRAS*, 222, 513

Whiteoak, J. B., & Wilson, W. E. 1990, *MNRAS* 245, 665

Fig. 1– Spectrum of the water maser emission from the nucleus of NGC 4945 made on 1995 October 13 at the Parkes radiotelescope of the CSIRO. The maser is variable on time scales of months but the spectrum shown is typical. The integration time is about 120 minutes (on and off source). The adopted heliocentric systemic velocity of the galaxy,  $561 \text{ km s}^{-1}$ , is indicated by the vertical bar. The dashed lines indicate the extremes of velocity that we observed with the VLBA. The solid bars above the velocity axis indicate the range of velocity within which maser emission is detected. The absolute gain calibration is accurate to  $\sim 30 \%$ . Velocities with respect to the Local Standard of Rest may be obtained from the relation  $V_{\text{LSR}} = V_{\text{hel}} - 4.6 \text{ km s}^{-1}$ .

Fig. 2– Sample plots of phase vs time for (*top*) the systemic maser feature at  $557 \text{ km s}^{-1}$  and (*bottom*) the red-shifted feature at  $665 \text{ km s}^{-1}$ . The phases sample a 24 hour sinusoid and are relative to the phase of the reference feature at  $699 \text{ km s}^{-1}$ . The right ascension and declination offsets of the maser features, with respect to the reference, were determined from these curves. The hour angle of the source with respect to the baseline is  $-8.5 \text{ h}$  at 12 UT.

Fig. 3– Map of the maser brightness distribution. The gray-scale shows velocity ( $414\text{--}719 \text{ km s}^{-1}$ ) with lighter shading indicative of more blue-shifted emission. The error bars reflect measurement noise at the  $3\sigma$  level. The position angle of the galactic disk is  $43 \pm 2^\circ$  (Dahlem et al., 1993). Marginal detections, for which the rms of the phase residuals from the model are  $> 1 \text{ rad}$ , are also not shown. The arrow indicated the maser feature closest to the systemic velocity of the galaxy.

Fig. 4– Position-velocity diagram for the maser emission. The impact parameter is measured with respect to the maser feature closest to the systemic velocity of the galaxy. The dashed line indicated the systemic velocity. The error bars represent position uncertainties at the  $3\sigma$  level.

Fig. 5– Comparison of various position determinations for the nucleus of NGC 4945. These include the new maser position reported here and the *a priori* position obtained by Batchelor et al., (1982) with the Parkes antenna, the interferometric position of H I absorption (Ables et al., 1987), the synthesis positions at 408 MHz (Large et al., 1981), 1.4 GHz (Ables et al., 1987), and 6.0 GHz (Whiteoak & Wilson 1990), and the position of the 1.6  $\mu\text{m}$  peak (Whiteoak & Gardner, unpublished). The sizes of the symbols correspond to the  $1\sigma$  uncertainties in position. The deconvolved angular size of the continuum source at 6 GHz is about  $6'' \times 2''$  (Whiteoak & Wilson 1990) at a position angle of  $\sim 45^\circ$  and is shown by the dashed ellipse. The position angle of the galactic disk is  $43 \pm 2^\circ$  (Dahlem et al., 1993).

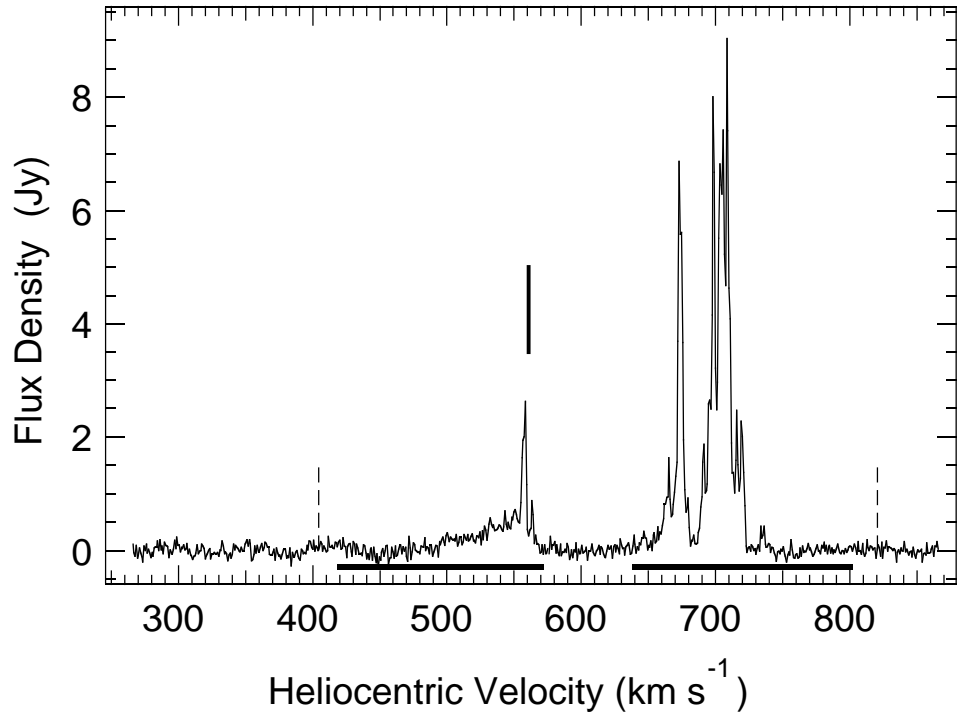


Fig. 1.— Greenhill et al.

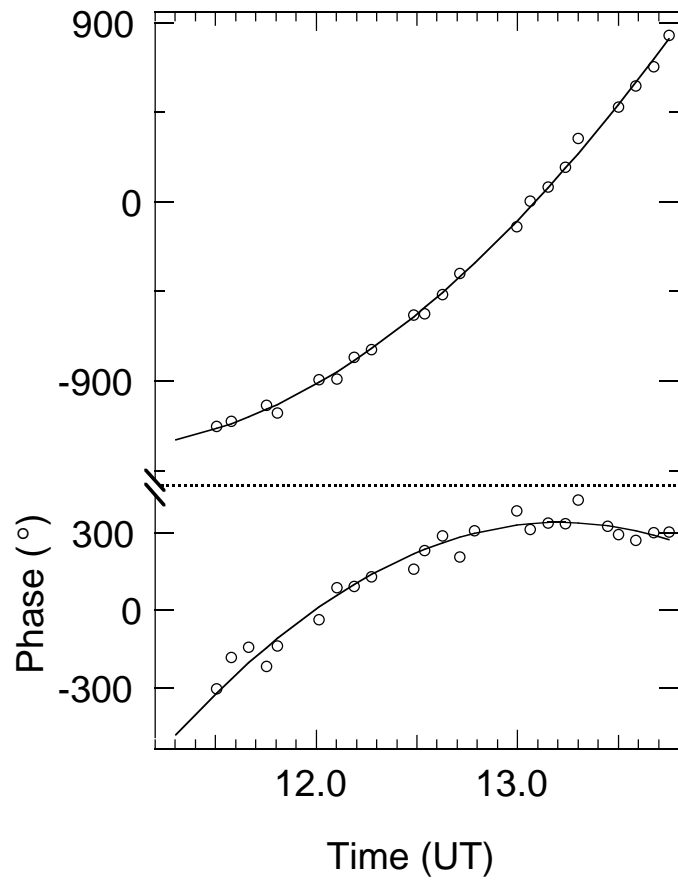


Fig. 2.— Greenhill et al.

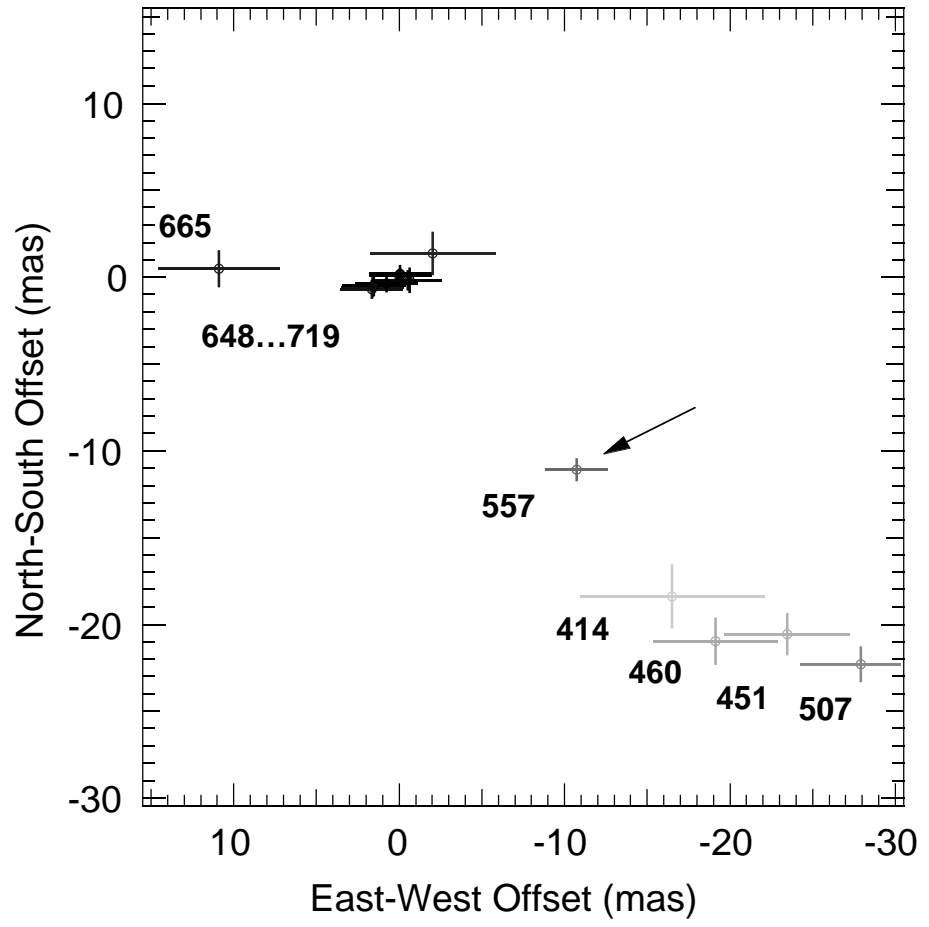


Fig. 3.— Greenhill et al.



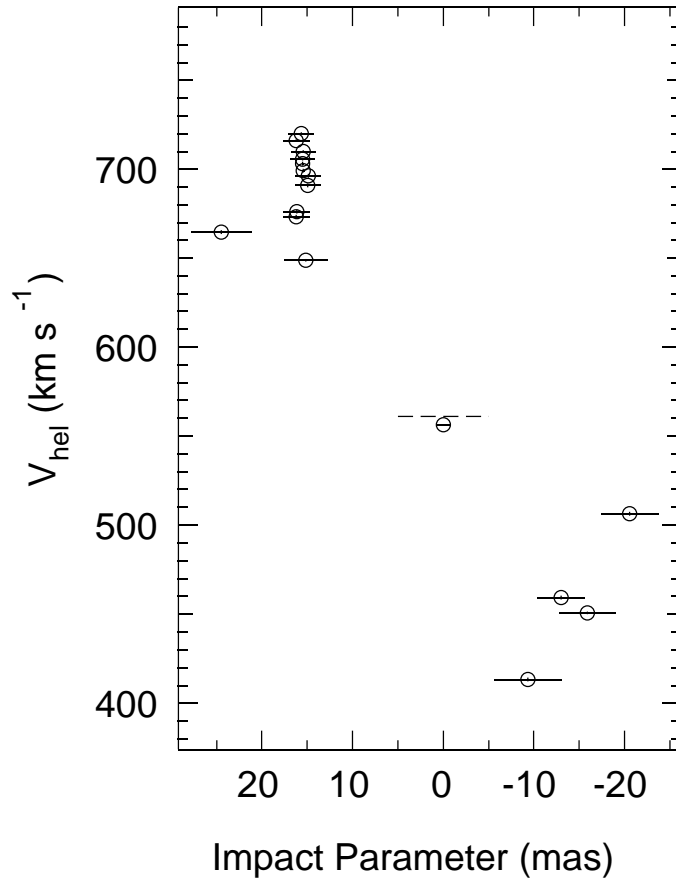


Fig. 4.— Greenhill et al.

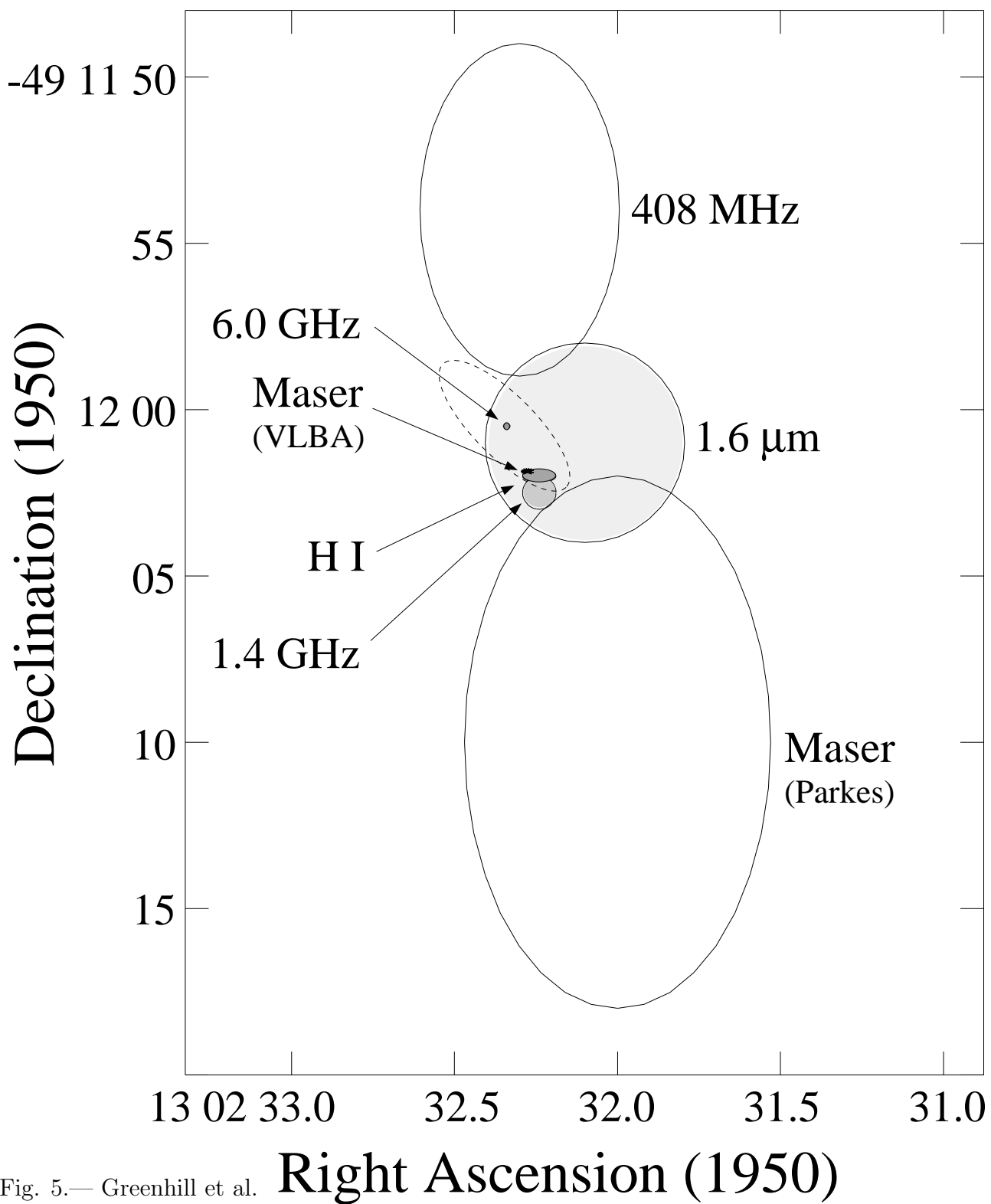


Fig. 5.— Greenhill et al.